

Detection of individual 0.4–28 μm wavelength photons via impurity-impact ionization in a solid-state photomultiplier

M. D. Petroff, M. G. Stapebroek, and W. A. Kleinhaus^{a)}

Rockwell International Science Center, 3370 Miraloma Avenue, Anaheim, California 92803

(Received 16 March 1987; accepted for publication 8 June 1987)

A solid-state device capable of continuous detection of individual photons in the wavelength range from 0.4 to 28 μm is described. Operated with a dc applied bias, its response to the absorption of incident photons consists of submicrosecond rise time pulses with amplitudes well above the electronic readout noise level. A counting quantum efficiency of over 30% has been demonstrated at a wavelength of 20 μm , and over 50% was observed in the visible-light region. Optimum photon-counting performance occurs for temperatures between 6 and 10 K and for count rates less than 10^{10} counts/s per cm^2 of detector area. The operating principle of the device is outlined and its performance characteristics as a photon detector are presented.

High quantum efficiency counting of individual photons is considered the ultimate sensitivity goal for detectors of visible and infrared light. As pointed out by Rose,¹ who examined the conditions for attaining this goal with photoconductive detectors, the minimum gain requirement is set by the thermal noise charge, $\sqrt{2kTC}/\pi$, where k is Boltzmann's constant, T is the temperature, and C is the total capacitance at the input of an ideal amplifier. A built-in detector gain of 200 to 300 is necessary even for a favorable case of $T \approx 10$ K and $C \approx 1$ pF. This requirement is satisfied by photomultiplier tubes which can be employed as photon counters for visible light, even at room temperature.² Solid-state devices, such as avalanche photodiodes (APD's),³ have shown some promise for photon counting for wavelength λ less than 2 μm because of the high gain inherent to their operation. While no APD's capable of single photon detection in a dc mode of operation have yet been found, several promising new approaches are being developed.⁴⁻⁶ APD's, in gated or reset operation, have been employed to detect single photons when biased above breakdown.^{7,8} Similar counting of photons has been reported using avalanche breakdown in metal-oxide-semiconductor structures.⁹ Other approaches, such as those involving up-conversion of photon energy to visible or near-infrared wavelengths, either in solid-state devices¹⁰ or in the more recent atomic-vapor quantum counter,¹¹ have failed to achieve adequate quantum efficiencies to be useful.¹²

In this letter, we report detection of individual photons with high counting quantum efficiency, η_c , for wavelengths from the visible-light region to $\lambda = 28 \mu\text{m}$ in the infrared. η_c is defined as the ratio of countable photon-detection events to the total number of incident photons. This has been accomplished with a solid-state device based on impurity-band conduction.¹³ When operated with a simple amplifier, photogeneration of a single carrier is detected as a submicrosecond rise time pulse with an amplitude well above the noise level. Each pulse has nearly equal amplitude for every photogenerated carrier and is the result of extremely fast internal charge amplification by impact ionization of impurity-band electrons. The mechanism provides very large and uniform

carrier multiplication factors in well localized and self-limiting avalanches. Photons absorbed simultaneously in different parts of the device create separate avalanches whose amplitudes are additive. With such photon response characteristics, it is appropriate to call these devices solid-state photomultipliers (SSPM's).¹⁴ SSPM's are, in effect, impurity-band avalanche photodiodes. However, impurity-band impact ionization is different from the usual valence-to-conduction-band impact ionization employed in APD's since only one carrier is capable of causing ionization. For the same semiconductor, impurity-band impact ionization occurs at much lower field strengths.

Device operation will be discussed in terms of existing n -type structures using arsenic-doped silicon (Si:As). The front-illuminated, single-crystal structure shown in Fig. 1(a) consists¹⁴ of a doped infrared-active layer (IRL) and a thin, undoped blocking layer (BL) grown epitaxially on a silicon substrate (SS) doped above the metal-insulator transition.¹⁵ The arsenic concentration in the IRL is about $5 \times 10^{17} \text{ cm}^{-3}$, sufficiently high for positively charged impurity-band carriers (D^+ charges) to have a drift mobility on the order of $1 \text{ cm}^2 \text{ V}^{-1} \text{ s}^{-1}$.¹⁶ An acceptor concentration in the range of $5 \times 10^{13} - 1 \times 10^{14} \text{ cm}^{-3}$ is provided in the IRL by counterdoping during epitaxial growth. A thin, transparent contact is formed in the BL by implantation of 3×10^{14} arsenic ions per cm^2 at an energy of 60 keV. As illustrated in Fig. 1, this device structure and appropriate bias conditions make possible the creation of localized avalanches in a thin ($\sim 4 \mu\text{m}$) high electric field region (gain

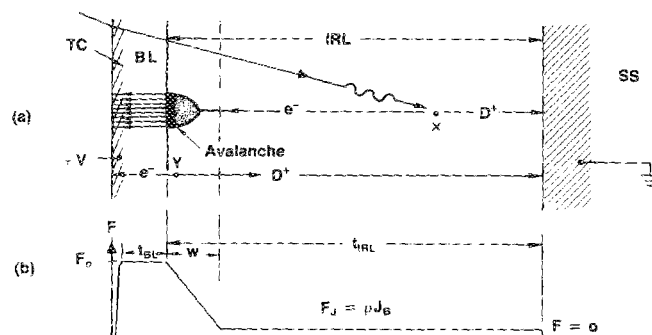


FIG. 1. (a) SSPM layer configuration with schematic representation of the generation of bias current and the effects following absorption of a photon. (b) Electric field profile.

^{a)} Present address: Optical Sciences Company, P. O. Box 1329, Placentia, CA 92670.

region) of the device, in response to photon absorption (and thermal generation) events in a thick ($\sim 25 \mu\text{m}$) low field region (drift region).

From charge neutrality, in the absence of an applied electric field, the concentration of D^- charges is equal to the total acceptor concentration, N_A , all of which are ionized. With the device at a temperature in the range of 6–10 K, application of a bias voltage of 7 V establishes the electric field profile shown in Fig. 1(b) by means of the effects discussed below. A constant field, $F_0 \approx 7 \times 10^3 \text{ V cm}^{-1}$, will appear in the BL (assumed to be free of any impurities). In the IRL, mobile D^+ charges are depleted away from the BL, leaving negative space charge due to fixed ionized acceptors (A^- charges). As a result, the field decreases linearly with distance into the IRL with a slope equal to $-eN_A/\epsilon\epsilon_0$, where e is the magnitude of the electron charge and $\epsilon\epsilon_0$ is the permittivity of silicon. The depletion width w is¹⁶

$$w = \sqrt{(2\epsilon\epsilon_0/eN_A) \{V - F_J(t_{\text{BL}} + t_{\text{IRL}})\} + t_{\text{BL}}^2} - t_{\text{BL}}, \quad (1)$$

where t_{BL} is the BL thickness, t_{IRL} is the IRL thickness, and F_J is the electric field induced in the undepleted part of the IRL by a bias current generated near the BL [e.g., at point Y in Fig. 1(a)] via field-assisted thermal ionization (the Poole-Frenkel effect¹⁷). The measured bias current density J_B of between 1 and $100 \mu\text{A cm}^{-2}$ and the IRL resistivity ρ of between 10^9 and $10^7 \Omega \text{ cm}$ requires, by Ohm's law, an electric field $F_J = \rho J_B$ of about 10^3 V cm^{-1} .

An electron- D^+ pair, created by an IR photon (or by thermal generation) at point X in Fig. 1(a), is separated by the field F_J . (A more complex process involving impact ionization by holes from the BL entering the IRL is involved for the visible-light response.) The electron drifts rapidly to the left, with a negligible probability for impact ionization while in the low field region, and the D^+ charge drifts more slowly to the right. An avalanche of well-defined gain, M ($\approx 4 \times 10^4$ at $V = 7 \text{ V}$ and $T = 7 \text{ K}$), occurs for each electron entering the steeply increasing electric field region adjacent to the BL. This is explained by the strong dependence of the impurity-impact ionization coefficient on field strength^{16,18} [i.e., $\alpha = \sigma N_D \exp(-F_c/F)$, where $\sigma \approx 1.6 \times 10^{-13} \text{ cm}^2$, N_D is the arsenic concentration, and $F_c \approx 7000 \text{ V/cm}$] combined with a limit to avalanche growth due to localized field collapse induced by space charge of the relatively immobile D^+ charges formed in the avalanche. Collection of the electrons is expected to occur in times on the order of a nanosecond. The achievable gain M depends on the field strength and is of the order of $M \approx A\epsilon\epsilon_0 F_0/e$, where A is the area over which the avalanche spreads.¹⁶ D^+ charges formed in the avalanche are incapable of ionizing neutral impurities because their energies are restricted to the narrow impurity band. They drift to the substrate in a few microseconds, where they are collected. The high impact-ionization gain does not apply to the electron- D^+ pairs responsible for the biasing current, which is generated preferentially in the highest field region close to the BL by field-assisted thermal emission. The electrons from these pairs cannot cause avalanches of large gain. Although the bias current may be larger than the average current due to the SSPM pulses, its contribution to the noise

current is very small because of the small gain.

Data, some of which are presented in this letter, were obtained with Si:As SSPM's with optically active areas between $0.005 \times 0.005 \text{ cm}^2$ and $0.1 \times 0.18 \text{ cm}^2$, including ten-element line arrays of $0.01 \times 0.025 \text{ cm}^2$ detectors. The devices were evaluated in a variable temperature, low-infrared-background, pinhole cryostat equipped with an InAs $3.2\text{-}\mu\text{m}$ wavelength light-emitting diode (LED) located about 10 cm from the SSPM and an optical fiber which permitted illumination with visible and near-infrared light from an external source. Radiation passing through the pinhole was attenuated and filtered by a cold bandpass filter. SSPM pulses were observed with simple transimpedance amplifiers (TIA's) external to the Dewar followed by further amplification. The amplified pulses were observed with an oscilloscope and counted or analyzed by other instruments.

The oscilloscope trace of Fig. 2(a) shows the detection of individual photons by a $0.01 \times 0.01 \text{ cm}^2$ SSPM for an incident photon-flux density of $2 \times 10^8 \text{ cm}^{-2} \text{ s}^{-1}$ at $\lambda = 20 \mu\text{m}$, as measured by a calibrated reference detector. Each pulse has approximately the same amplitude well above the noise level. Occasionally, larger pulses occur when two photons are detected within a time less than the amplifier-limited pulse width (amplifier bandwidth is 100 kHz in this case). At $T = 7 \text{ K}$ and $V = 7.5 \text{ V}$ [see Fig. 2(a)], about 10% of the pulses are dark pulses, each of which is due to thermal generation of a carrier in the active volume of the device. Dark pulses are indistinguishable from photon pulses and are observed when the pinhole is closed and the photon-flux density inside the cryostat cold chamber is well below the $10^6 \text{ cm}^{-2} \text{ s}^{-1}$ measurement limit of the reference detector.

The average pulse rate minus the dark count rate, at a given temperature and bias, is proportional to the average number of incident photons as long as the number of counts per second per unit area is below a temperature-dependent, saturation-count-rate density. Saturation is attributed to a drop of the local electric field in the gain region due to trapping of a small fraction of the avalanche D^+ charges next to fixed A^- sites in the low field region.¹⁶ The affected area is estimated to be about $2 \times 10^{-6} \text{ cm}^2$ from experimental data on the saturation-count-rate density and on the relaxation time of the trapped charge. At $T = 7 \text{ K}$, the measured relaxation time is about $50 \mu\text{s}$.

A more dramatic demonstration of individual photon detection is provided by the response of the SSPM to very short-duration bursts of $\lambda = 3.2 \mu\text{m}$ photons generated by the LED, as shown in Figs. 2(b) and 2(c). The top oscilloscope traces in these two photos show short ($< 0.1 \mu\text{s}$) voltage pulses applied to the LED at a repetition rate of $10\,000 \text{ s}^{-1}$. The bottom traces show the resulting superposition of SSPM outputs. In Fig. 2(b), the average number of photons detected (deflected traces) per burst from the LED is about 0.2, as determined by a pulse counter. Comparison of intensities between deflected and undeflected traces is consistent with this ratio. (The observed delay between the LED burst and the start of the SSPM pulses and their pulse shape are entirely due to amplifier characteristics.) Figure 2(c) shows the effect of an increase in the number of photons emitted per

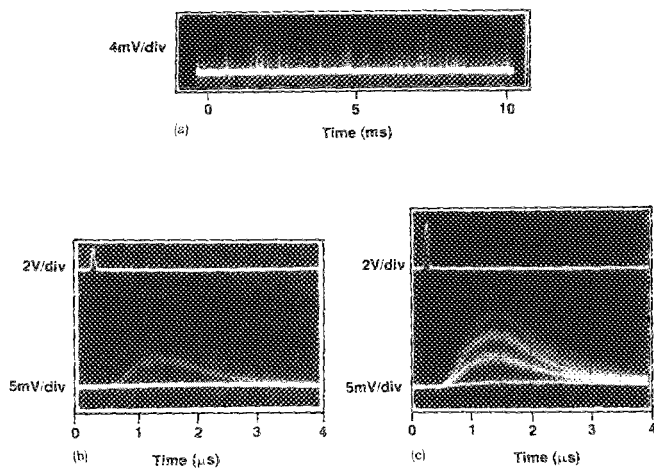


FIG. 2. Oscilloscope traces showing SSPM output pulses. (a) Single trace with pulses from detection of $\lambda = 20 \mu\text{m}$ photons. (b) and (c) Multiple traces. The top traces display voltage impulses applied to the LED to produce bursts of $3.2 \mu\text{m}$ photons. The bottom traces show the corresponding amplified SSPM output. About 0.2 photons/burst are detected in (b) and about 1.5 photons/burst are detected in (c).

LED burst so that an average of 1.5 photons per burst is detected. Here, several bands of pulse amplitudes are observed. The first deflected band corresponds to one photon detected per LED burst, the second corresponds to two photons, and the fainter third band of pulses is formed when three photons are detected simultaneously within a fraction of the amplifier time constant. More quantitative measurements of SSPM pulse amplitudes using a multichannel pulse height analyzer verified that their occurrence rate follows the expected Poisson distribution for randomly occurring photon absorption events. These data, and similar data using a faster amplifier with 5 MHz bandwidth, conclusively prove that SSPM's are true single-photon detectors with submicrosecond response to photon incidence.

Several important performance characteristics are presented in Fig. 3 from data obtained on a $0.01 \times 0.01 \text{ cm}^2$ SSPM. Figure 3(a) shows that the dark- and saturation-count-rate densities are strong functions of temperature, as

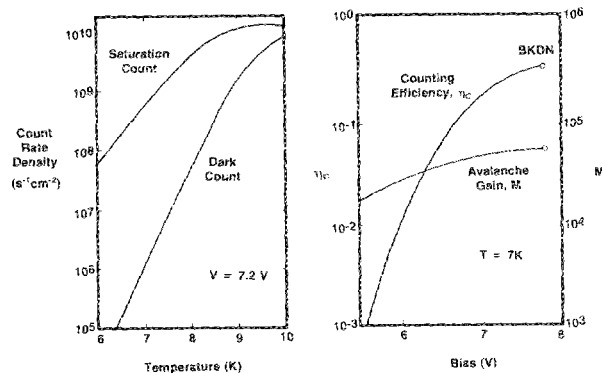


FIG. 3. (a) Temperature dependence of the SSPM dark- and saturation-count-rate densities. (b) Bias dependence of gain, M , and counting quantum efficiency, η_c ($\lambda = 20 \mu\text{m}$).

expected for thermally activated processes. Figure 3(b) gives the measured η_c at $\lambda = 20 \mu\text{m}$ and gain at a temperature of 7 K as a function of bias. The strong dependence of η_c on applied voltage above 5 V is explained by the pronounced effect of voltage on the electric field F_j in the IRL which determines the probability of photoelectrons reaching the gain region.¹⁶ The slow variation of gain with bias is due to the relatively small effect of bias voltage above 5 V on the high electric field in the gain region.

The spectral dependence of η_c in the IR region was measured with LED's ($\lambda = 0.9, 3.2 \mu\text{m}$) and a black-body source with bandpass filters ($\lambda = 4.5, 10, 15, 20 \mu\text{m}$) calibrated with a reference detector of known spectral response. In the visible-light region, η_c was determined by light from a monochromator calibrated with a silicon photodiode of known spectral quantum efficiency.¹⁹ The spectral response has a maximum $\eta_c > 0.5$ in the visible region, then drops to about $\eta_c = 0.03$ at $\lambda = 1.1 \mu\text{m}$, rising again to about $\eta_c = 0.3$ at $\lambda = 20 \mu\text{m}$. This behavior has been adequately explained in terms of the known intrinsic and extrinsic absorption coefficients of the Si:As material.¹⁶

It is a pleasure to thank J. G. Quetsch for growth of the material, L. M. Squillace and A. G. Crouse for device processing and preparation, and R. Bharat for many helpful discussions during the course of this work.

- ¹A. Rose, in *Proceedings of the 3rd International Conference on Photoconductors*, Stanford, CA Aug. 1969, published as a supplement to J. Phys. Chem. Solids, edited by E. M. Pell (Pergamon, Oxford, 1971), p. 7.
- ²D. V. O'Connor and D. Phillips, *Time-Correlated Single Photon Counting* (Academic, New York, 1984).
- ³F. Capasso, in *Semiconductors and Semimetals*, edited by R. K. Willardson and A. C. Beer (Academic, New York, 1985), Vol. 22, Part D, p. 2.
- ⁴F. Capasso, W. T. Tsang, and G. F. Williams, *IEEE Trans. Electron Devices* **ED-30**, 381 (1983).
- ⁵F. Capasso, J. Allam, A. Y. Cho, K. Mohammed, R. J. Malik, A. L. Hutchinson, and D. Sivco, *Appl. Phys. Lett.* **48**, 1294 (1986).
- ⁶J. Allam, F. Capasso, K. Alavi, and A. Y. Cho, *IEEE Electron Device Lett.* **EDL-8**, 4 (1987).
- ⁷T. E. Ingerson, R. J. Kearney, and R. L. Couiter, *Appl. Opt.* **22**, 2013 (1983).
- ⁸B. F. Levine and C. G. Bethea, *Appl. Phys. Lett.* **44**, 553 (1984).
- ⁹T. P. Lester and D. L. Puffrey, *IEEE Trans. Electron Devices* **ED-31**, 1420 (1984).
- ¹⁰N. Bloembergen, *Phys. Rev. Lett.* **2**, 84 (1959).
- ¹¹J. A. Gelbwachs, C. F. Klein, and J. E. Wessel, *IEEE J. Quantum Electron.* **QE-14**, 77 (1978).
- ¹²P. L. Richards and L. T. Greenberg, *Infrared and Millimeter Waves* **6**, 149 (1981).
- ¹³N. F. Mott and W. D. Twose, *Adv. Phys.* **10**, 107 (1961).
- ¹⁴M. D. Petroff, M. G. Stapelbroek, and W. A. Kleinmans, U.S. Patent No. 4 586 068 (29 April 1986).
- ¹⁵N. F. Mott and E. A. Davis, *Electronic Processes in Non-Crystalline Materials* (Clarendon, Oxford, 1979).
- ¹⁶M. D. Petroff and M. G. Stapelbroek (unpublished).
- ¹⁷A. G. Milnes, *Deep Impurities in Semiconductors* (Wiley, New York, 1973).
- ¹⁸S. M. Sze, *Physics of Semiconductor Devices*, 2nd ed. (Wiley-Interscience, New York, 1981), p. 45.
- ¹⁹The photodiode and calibration were generously provided by J. Geist, National Bureau of Standards, Gaithersburg, MD 20899.